Direct Voltammetric Observation of Reversible and Irreversible Oxidations of Two-Dimensional J-Aggregates of Cyanine Dye

Mitsuo Kawasaki* and Tomoo Sato

Department of Molecular Engineering, Graduate School of Engineering, Kyoto University, Yoshida, Kyoto 606-8501, Japan

Received: June 27, 2000; In Final Form: October 18, 2000

The redox properties of two-dimensional (2D) J-aggregates of a typical thiacarbocyanine dye have been studied directly by the standard electrochemical method in conjunction with the recently developed technique for controlled layering of 2D J-aggregates on a self-assembled cysteamine monolayer on an atomically flat Au(111). The cyclic voltammograms measured at widely ranging scan rates from 10 mV/s to 100 V/s illuminated unique mechanistic features of the J-aggregate oxidation, which proved to be a convolution of reversible and irreversible oxidations involving the charge transfer of up to 4 electrons/molecule. The oxidation-induced irreversible bleaching of the J-band was accompanied by negligibly small changes in its peak position and sharpness, suggesting that the irreversible reaction occurs preferentially along the domain edges or boundaries. The two different phases of oxidation could be more or less clearly separated under the fast scan mode (scan rate larger than ∼10 V/s), giving us the unprecedented opportunity to directly observe the partial reversible oxidation of the 2D J-aggregate involving a limited amount of charge-transfer much less (∼15%) than that of the hypothetical one-electron oxidation of all dye molecules. This limitation probably represents energetic constraint against the accumulation of too many repulsive positive holes. For a series of J-aggregates partitioned into progressively smaller segments with a coadsorbed diluent dye, the corresponding reversible potentials were 0.18−0.10 V more negative than that expected for the monomer. The results indicate that the J-aggregation caused concurrent upward and downward shifts in the dye HOMO and LUMO levels, respectively. The way the J-aggregation changes the redox levels depends critically on the nature of positive holes in the given aggregate framework.

1. Introduction

The J-aggregate of cyanine dyes is a unique molecular assembly characterized by an extraordinary sharp absorption and a resonance fluorescence that markedly red-shifted from the monomer band, and it has stimulated extensive studies of related physics and chemistry by many research groups in different disciplines.[1−5] Practically, the J-aggregate has served as an important spectral sensitizer in silver halide photographic materials,[5,6] as the electronically excited J-aggregate can effectively inject photoelectrons into the conduction band of AgX and its sharp absorption band allows easier control over the spectral sensitivity of the photoimaging system. For such J-aggregates that are directly adsorbed on the solid surface, the most fundamental parameters for the electron transfer phenomena are the energetic positions of the dye HOMO and LUMO levels. Experimentally, these molecular orbital levels of adsorbed dye molecules have been estimated indirectly on the basis of electrochemical redox potential data, which are typically measured (preferably by using the phase-sensitive second harmonic voltammetry method to obtain the reversible potential data[7,8]) for monomeric dyes dissolved in nonaqueous solutions. There is no doubt, however, that the experimental information concerning the monomeric dyes in solution immediately loses its absolute meaning for the electron transfer phenomena involving the aggregated dyes. In particular the spectral properties of J-aggregates are markedly different from that of the monomeric state, and thus, the individual HOMO and LUMO levels must also be affected accordingly by the J-aggregation.

So far, the only sophisticated work that experimentally addressed the above question is that of Lenhard and Hein.[9] They used a structurally rigidized thiadicarbocyanine dye (red sensitizing) adsorbed on cubic AgBr microcrystals embedded in a gelatin matrix, where they found that both the monomeric dye and the J-aggregate could undergo a reversible one-electron oxidation reaction when treated by a series of redox buffer solutions. By analyzing the extent of oxidation as a function of the buffer potential in the framework of the standard Nernst equation, they concluded that the formal oxidation potential (HOMO) of the J-aggregate was 74 mV more positive (lower) than that of the monomer. This means that the J-aggregation (causing for the given dye a ∼0.25 eV red shift in the HOMO−LUMO transition energy) produced a much larger downward shift of the LUMO level. Lenhard and Hein also suggested for their J-aggregate that the holes (radical dications) produced in the one-electron oxidation process had a far slower mobility than that of an exciton. This is another interesting question that may be closely related to the changes of redox levels by J-aggregation.

In this paper, we introduce an apparently more direct experimental approach to the above issues by making use of a remarkably uniform two-dimensional (2D) J-aggregate monolayer of an anionic thiacarbocyanine dye. We have recently found that it can be very successfully layered on top of a self-assembled cysteamine monolayer on an atomically flat Au(111)

* Corresponding author. FAX: (+81)75-753-5540. E-Mail: kawasaki@ap6.kuic.kyoto-u.ac.jp.

10.1021/jp002309a CCC: $20.00
Published on Web 12/30/2000

surface.[10,11] Similar cysteamine monolayers on gold, providing a densely amino-group-functionalized surface, have widely been utilized for preparation of chemically modified or redox-modified gold electrodes.[12−18] In the present case, the dye moiety is held at a fixed position ~13 Å above the metal (Au) surface, and the interface electron transfer through this significant tunneling gap can be followed in situ under facile electrochemical control of the energetic position of the dye HOMO level relative to the Fermi level of the Au(111) substrate. Besides, the fundamental electrochemical processes in question involve no diffusion problems in the electrolyte solution. In such a diffusionless system, the current−potential profiles obtained by the linear-sweep or cyclic voltammetry provide more straightforward information about the electron-transfer kinetics at the given electrode.[19−21] Our samples thus serve as a superior model electrode system for directly investigating the redox properties of layered J-aggregates, although a concurrent investigation of the reduction potential is not feasible because of the interruptive reductive desorption of thiolates (dissociation of S−Au bonds)[22,23] in the corresponding far negative potential region.

The thiacarbocyanine dye we have studied is not at all special and readily undergoes an irreversible oxidation process as the majority of other cyanine dyes.[7] Nonetheless, a considerably fast-scan voltammetry reaching 100 V/s at maximum allowed us to observe for the first time the reversible or quasi-reversible voltammograms for layered J-aggregates. We show that the J-aggregation in our model system, as opposed to that studied by Lenhard and Hein,[9] causes a net negative (upward) shift in the reversible oxidation potential (HOMO). The energetics that gives us a rationale for this trend is discussed along with other mechanistic implications.

2. Experimental Section

2.1. Materials and Sample Preparation. Two anionic cyanine dyes, 5,5′-dichloro-3,3′-disulfopropyl-9-ethylthiacarbocyanine triethylamine (Dye 1) and 5,5′-dichloro-3,3′-disulfopropyl-9-ethylthiacyanine triethylamine (Dye 2), were kindly supplied by Dr. Rene De Keyzer (Agfa Gevaert N. V., Belgium). The focus in this study is on the J-aggregate of Dye 1. Dye 2 was used as an effective diluent, which by being coadsorbed with Dye 1 produces less-ordered Dye 1 J-aggregates with smaller domain sizes. These dyes were used in the form of typically 0.1 mM solution (including mixed solution of Dye 1 and Dye 2) in mixed water and ethanol solvent of 1:1 volume ratio. Cysteamine (CA), or 2-mercaptoethylamine hydrochloride, was purchased from Wako Pure Chemical Industry, Ltd. and used in the form of 10 mM solution in ethanol (guaranteed reagent grade). Figure 1 shows the molecular structures of the sample dyes together with that of CA.

An atomically flat, high-quality Au(111) film, approximately 250 nm thick, was prepared on freshly cleaved natural mica (purchased from The Nilaco Corporation) using the DC Ar-ion sputtering method as described in detail elsewhere.[24−26] The Au(111) film prepared in this way has an extensively terraced (111) texture with each atomic terrace spanning hundreds of nm in width.

The self-assembled monolayer of CA was formed by immersing the Au(111) substrate in the given ethanolic solution for ~5 min at room temperature (~20 °C), followed by rinsing with running ethanol. The dye adsorption onto the CA-covered Au(111) was allowed for typically 5 min at ~50 °C from the 0.1 mM dye solution. The dyed sample was quickly rinsed by running water and dried in air after visible water droplets had been blown off by nitrogen.

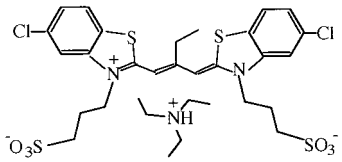

Dye 1

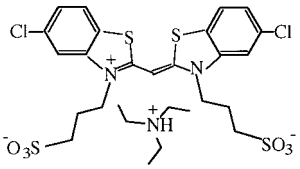

Dye 2

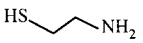

Cysteamine (CA)

Figure 1. Structures of cyanine dyes and cysteamine hydrochloride (CA) used in this work.

2.2. Absorption Spectroscopy. The absorption spectra of the dye aggregate monolayers prepared on the highly reflective Au(111) substrate were measured in the reflection mode (at normal incidence) by using a spectromicroscope comprising a multichannel analyzer PMA-11 (Hamamatsu Photonics Co.) and a Nikon microscope. The microscope was operated at the lowest magnification of ×10, where the sampling spot diameter was approximately 0.25 mm. The spectra were recorded in terms of the reflection absorbance defined by $\log(R_0/R)$, where R and R_0 represent the measured reflectance of the sample with and without the adsorbed dye, respectively.

2.3. Voltammetry. All the electrochemical measurements were carried out at room temperature (~20 °C) in a three-electrode cell, ~25 mm in diameter and ~50 mm in height, accommodating approximately 20 mL of a concentrated aqueous electrolyte (1.5 M KNO_3). The working electrode potential was controlled with a scanning potentiostat (Hokuto Denko Corporation, model HA-501) in combination with an external function generator (Hokuto Denko Corporation, model HB-107A), relative to an Ag/AgCl/NaCl(3M) reference electrode (The B. A. S. Corporation, model RE−1B). The counter electrode was a Pt wire 0.5 mm in diameter. The working electrode, the dye/CA-covered Au(111) film on mica, was cut to the size of typically ~4 × 20 mm^2, of which the 1−5 mm (depending on the current level) end portion was brought into the electrolyte. The pH of the nonbuffered KNO_3 solution was in the range of 6−7. The dissolved oxygen in the electrolyte was removed by N_2 gas bubbling before each experimental run. The current−potential profiles were measured at various potential scan rates ranging from 10 mV/s to 100 V/s and recorded in a personal computer for further data processing.

2.4. X-ray Photoelectron Spectroscopy (XPS). The XPS data were taken in an ESCA-750 spectrometer (Shimadzu Corp.) with Mg Kα radiation of 1253.6 eV for samples typically ~6 × 6 mm^2 in area at the standard photoemission angle of 90°.

3. Results and Discussion

3.1. Spectral Property and Structure of 2D J-Aggregate on CA-Covered Au(111). As discussed in detail elsewhere,[10,11] a highest-quality 2D J-aggregate with an extraordinary sharp J-band forms preferentially on a densest but still not fully ordered CA monolayer at a considerably high temperature (~50 °C) of dye adsorption. Spectrum a in Figure 2a represents such a sharp J-band (peaked at 657 nm and red-shifted by more than

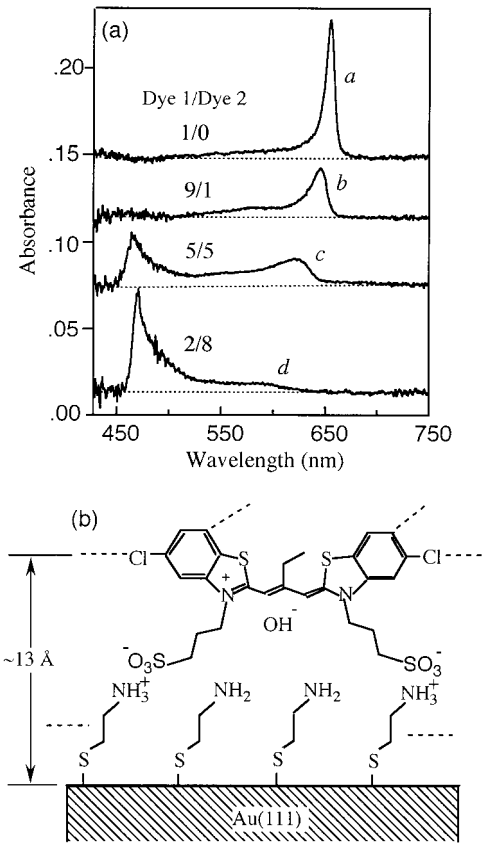

Figure 2. (a) Series of absorption spectra of 2D J-aggregates of Dye 1 layered on top of a self-assembled cysteamine monolayer on Au(111). Coadsorption of a diluent dye (Dye 2) from mixed-dye solutions with Dye 1/Dye 2 molar ratios of 9/1 (b), 5/5 (c), and 2/8 (d) causes systematic blue shift and broadening of the J-band from that (a) obtained without coadsorption of Dye 2. (b) A cross-sectional model of the bilayered structure consisting of 2D J-aggregate of Dye 1 and cysteamine monolayer on Au(111).

100 nm from the monomer absorption peak at ~550 nm) of Dye 1 J-aggregate prepared in this manner. Figure 2a also includes a series of absorption spectra obtained for smaller and less perfectly ordered Dye 1 J-aggregates adsorbed from mixed-dye solutions of Dye 1 and Dye 2 with various mixing ratios. In agreement with the previously reported dilution or co-aggregation experiments,[9,27,28] the partition of Dye 1 J-aggregate by the coadsorbed diluent dye (Dye 2) caused systematic blue shift and peak broadening of the Dye 1 J-band; thereby, the Dye 1 monomer absorption at ~550 nm also became more distinct. Of course, at much higher mixing ratios of Dye 2, its own J-band at ~470 nm[29] became overwhelmingly the strongest. Also, the change of the integral intensity of the Dye 1 absorption bands with increasing mixing of Dye 2 suggests that the two dyes were adsorbed with approximately the same molar ratio as that in solution. We hereafter use the molar mixing ratio in solution as the approximate dye composition to specify the level of co-aggregation between Dye 1 and Dye 2.

Figure 2b is a cross-sectional diagram of the bilayered dye/CA assembly, as inferred through a detailed interface analysis by the XPS method.[11] The individual dye molecules in this structure are doubly linked to the surface amino groups with ammonium sulfonate bonds, and the excess positive charge associated with the monocationic dye chromophore is most likely compensated by incorporating hydroxide ions from the dye solvent.[11] In the geometry of Figure 2b, the 3,3′-disulfopropyl substituents, in cooperation with the CA monolayer, support the 2D J-aggregate monolayer at a fixed distance above

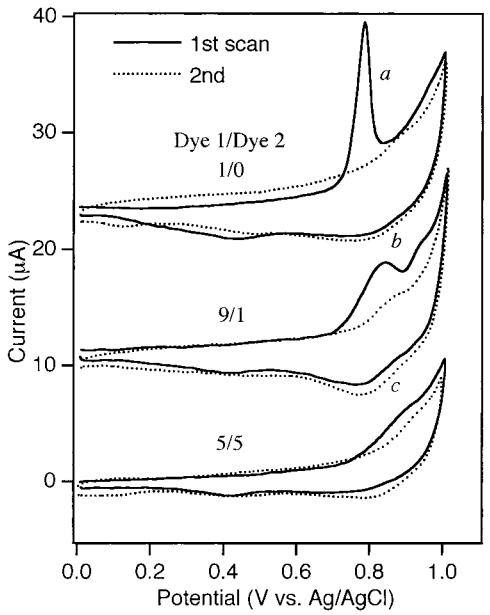

Figure 3. Cyclic voltammograms for a series of Dye 1 J-aggregates with (b and c) and without (a) coadsorption of Dye 2 measured at a considerably slow scan rate of 25 mV/s. The scan was started at 0 V in the anodic direction. Solid and dotted lines represent first- and second-scan voltammograms, respectively.

the Au(111) surface. The exact distance depends on the presently unknown tilt angles of the supporting alkyl chains, but we roughly estimate it to be around ~13 Å.

3.2. Irreversible Oxidation of J-aggregate. We first analyze the cyclic voltammograms obtained at relatively small scan rates below 1 V/s to illuminate some important characteristics of the irreversible oxidation of the 2D J-aggregate. Figure 3 shows typical examples obtained at scan rate of 25 mV/s for various J-aggregates of Dye 1 with and without the coadsorption of Dye 2. The oxidation potential of Dye 2 (thiacyanine) is expected to be so positive[7] that all the peaks observed within the selected scan window are either associated with Dye 1 or due to the redox reactions involving the Au(111) substrate (gold oxide formation and removal). Depending on the scan rate, the latter caused a steeply rising anodic current in the region near the switching potential (~1 V in Figure 3; the scan was always started at 0 V to the anodic direction) following the reversed scan by the oxide removal peaks (mainly at around ~0.8 V in the scan condition of Figure 3). Similar peaks arising from the gold oxide formation and removal, suggesting that the gold surface was not fully passivated by the overlying monolayers, were observed in the absence of the 2D J-aggregate as well and have also been reported for gold electrodes covered with much longer-chain alkanethiol monolayers.[30,31]

In Figure 3, the highest-quality 2D J-aggregate with the sharpest J-band gives an exceptionally sharp oxidation peak at 0.79 V during the first anodic scan. The reverse scan gives no corresponding cathodic peak, and the anodic peak completely disappears for repeated scans, so the observed oxidation is totally irreversible. With increasing scan rate, the position of this anodic peak shifted from 0.74 V at 10 mV/s to 0.88 V at 1 V/s. The sharp anodic peak also facilitates determination of the integral current density, or the total charge per unit area that the 2D J-aggregate has given up to the gold electrode. The thus estimated value is 8.0×10^{-5} C/cm^2, or 5.0×10^{14} electrons/cm^2. Comparing this value with the absolute dye coverage, 1.3×10^{14} molecules/cm^2 (measured by the ethanolic extraction method[10,11]), we find that each dye molecule has given up a

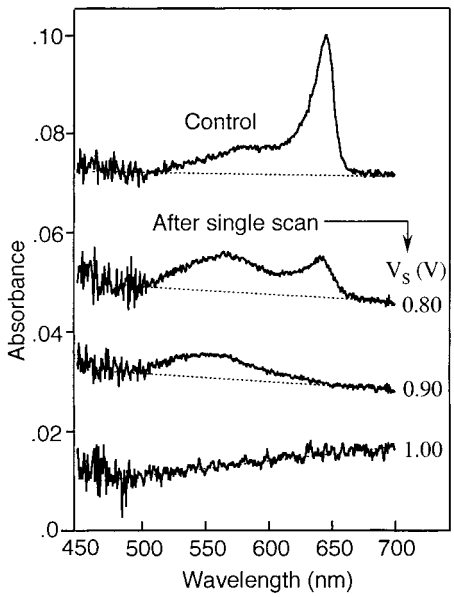

Figure 4. Absorption spectra of 2D J-aggregate of Dye 1 (prepared from mixed-dye solution with Dye 1/Dye2 molar ratio of 9/1) taken after a single voltammetric scan at 25 mV/s with varied switching potentials, V_s, indicating that anodic bleaching of the monomer band (~550 nm) occurs in a more positive potential region above 0.9 V than that required to bleach the J-band.

total of 4 electrons in the irreversible oxidation process. The resulting changes in the dye molecular structure are difficult to specify at present, but the XPS spectra taken after the anodic scan at least suggests that the irreversibly oxidized dye remains are something that easily come off the electrode surface into the electrolyte solution.[32]

Figure 3 demonstrates two other important features of the irreversible J-aggregate oxidation in the slow scan mode: i.e., a strong broadening or flattening of the anodic peak for the lower-quality Dye 1 J-aggregates and an apparent splitting of the anodic peak that is most clearly resolved in the middle voltammogram. The intentional segmentation of the Dye 1 J-aggregate by the coadsorbed diluent dye will probably lead to a higher degree of site heterogeneity, which at first seems to be a likely cause of the remarkable changes in the anodic peak shape. However, as for the extensive broadening of the anodic peak, we will show later that this interpretation is not correct, the real cause being more intimately correlated with the kinetics of the irreversible oxidation reaction. On the other hand, the observed splitting of the anodic peak is in fact related to a kind of site heterogeneity that allows some fraction of Dye 1 to be isolated as monomers in the mixed-aggregate framework. Indeed, the split higher-potential sub peak is located at ~0.95 V, which is close to the reversible monomer oxidation potential (0.95−0.98 V)[7,8] in acetonitrile solution reported for a cationic thiacarbocyanine dye with exactly the same chromophore structure as that of Dye 1. Furthermore, a series of absorption spectra shown in Figure 4 gives us a convincing proof for this correlation.

The spectra in Figure 4 (except for the control) were taken immediately after a single voltammetric scan at 25 mV/s with some different switching potentials (V_s). The sample is the 9/1 mixed aggregate for which the splitting of the anodic peak was most clearly observed in Figure 3. With $V_s = 0.80$ V, near the broadened main anodic peak at ~0.83 V, the J-band already undergoes a significant drop in intensity. It almost disappears with $V_s = 0.90$ V, while the monomer absorption (around ~550 nm) still survives since the anodic scan was reversed before

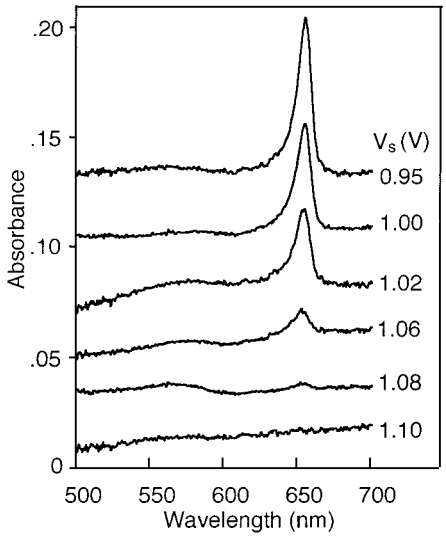

Figure 5. Series of absorption spectra taken for the highest-quality 2D J-aggregate of Dye 1 after a single voltammetric scan at 100 V/s with various switching potentials. Anodic bleaching of the J-band is accompanied by almost no changes of peak position and peak width.

entering the region of monomer oxidation. Of course, the residual monomers at this stage partly include those which were dissociated from the J-aggregates by their irreversible oxidation. This does not influence at all, however, the fact that monomers can survive a more positive potential. Further increasing V_s beyond the sub peak to 1.0 V then also eliminates the monomer absorption as expected. The fraction of isolated Dye 1 monomers must of course increase with increasing mixing ratio of Dye 2, but the more serious broadening or flattening of the J-aggregate oxidation peak (see the bottom voltammogram in Figure 3) also blurs out the monomer oxidation signal. Though within the framework of irreversible oxidation phenomena, the results indicate that the monomers are more difficult to oxidize than the J-aggregate. This is also consistent with the reversible oxidation potential of the 2D J-aggregate and its domain-size dependence, as discussed in the following section.

Figure 4 also provides a useful additional hint concerning a marked site preference in the irreversible oxidation reaction. Namely, the oxidation-induced bleaching of the J-band appears to cause a minor shift in its peak position. This is quite a general feature associated with the irreversible oxidation, as strengthened with another series of absorption spectra, Figure 5, taken for the highest-quality J-aggregate after a single voltammetric scan at the maximum scan rate of 100 V/s. It can be seen that a large intensity decrease in the corresponding sharpest J-band to less than 10% of the original intensity is accompanied by negligibly small changes of the peak position and sharpness. This is impossible if the respective dye molecules in each J-aggregate domain underwent the irreversible oxidation randomly without any site preference, thereby breaking up the original J-aggregate domain into a number of smaller segments. This must be accompanied by significant peak broadening and blue shift in the J-band (cf. Figure 2). Figure 5 thus strongly suggests that the irreversible oxidation reaction occurs highly preferentially along the domain edges or boundaries. Then insofar as the original domain size is sufficiently large, the irreversible oxidation of even more than 90 % of the total dye molecules leaves J-aggregates that have considerably shrunken but still consist of a large enough number of molecules to preserve an equally sharp J-band. This is exactly what is observed in Figure 5; a feature that closely resembles the way the J-band is diminished when the 2D J-aggregate is subjected

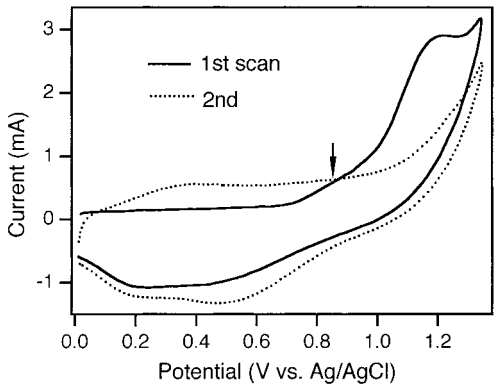

Figure 6. Wide-scan voltammogram for the highest-quality 2D J-aggregate of Dye 1 obtained in the fast scan condition of 100 V/s. In the first anodic scan, a small shoulder-like signal (indicated by an arrow) appears in advance of a large anodic current due to irreversible oxidation.

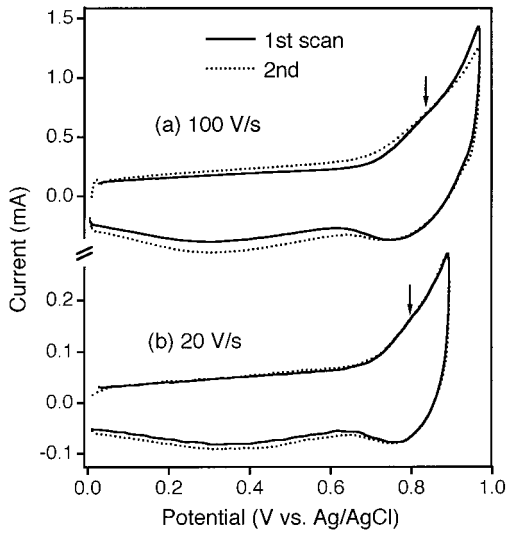

Figure 7. Examples of fast-scan (100 and 20 V/s) reversible voltammograms for the highest-quality 2D J-aggregate of Dye 1 observed by using a narrower potential window than in Figure 6. A well-defined cathodic peak now shows up in the reverse scan. Arrows indicate the position of shoulder-like reversible anodic signal.

to dissolution in plain solvent.[28] Both irreversible oxidation and simple dissolution of an interior dye molecule lead to an identical result breaking up the otherwise homogeneous J-aggregate structure and are thus strongly disfavored energetically.

3.3. Reversible Oxidation under Fast-Scan Mode. In the region of potential sweep rate above ~10 V/s, the sharp 4-electron oxidation peak for the highest-quality 2D J-aggregate in the slow scan mode was taken over by such a characteristic wave as shown in Figure 6, in which a small anodic current (a shoulder indicated by arrow) associated with the initial step of oxidation is noticeably separated from a large signal arising from the follow-up irreversible oxidation. By switching the anodic scan before the onset of this large irreversible current, we then found that the initial step of oxidation could be made reversible or quasi-reversible; thereby, a well-defined cathodic peak showed up in the reverse (cathodic) scan. Typical examples are shown in Figure 7 for two different scan rates, 100 V/s and 20 V/s. It can be seen that the cathodic peak (with 0.1−0.15 V fwhm) position is almost invariant at 0.77−0.78 V for the given range of scan rates. The integral current density under this cathodic peak was estimated to be at most $\sim 2 \times 10^{-6}$ C/cm^2, or $\sim 1.5 \times 10^{13}$ electrons/cm^2, which means that the reversible oxidation and reduction cycle observed in Figure 7 involves a charge-transfer much less (~15%) than 1 electron/molecule, in marked contrast with the irreversible oxidation. It should be also noted that we found no such reversible nor quasireversible waves in the absence of the 2D J-aggregate. Thus, the cathodic peak in Figure 7 should be strictly discriminated from the gold oxide removal peak mentioned earlier.

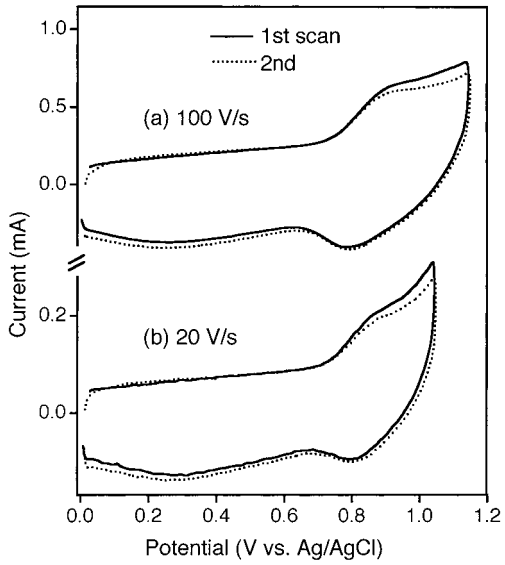

Figure 8. As in Figure 7 but for a lower-quality 2D J-aggregate of Dye 1 prepared at Dye 1/Dye2 mixing ratio of 5/5. Instead of shoulder-like anodic signals in Figure 7, reversible voltammograms here exhibit a distinct anodic peak along with a cathodic peak.

In the case of the highest-quality 2D J-aggregate, the reversible anodic signal that must be coupled with the cathodic peak is still significantly overlapped with the tail of a far stronger signal associated with the irreversible oxidation, thus exhibiting a shoulder-like feature at best. This anodic shoulder can be located at ~0.83 V (only ~60 mV apart from the cathodic peak) for a scan rate of 100 V/s (Figure 7a; see also Figure 6) and, unlike the cathodic peak, noticeably shifted in the negative direction with decreasing scan rate so as to almost coincide with the cathodic peak at ~0.78 V for scan rates of 20 V/s or less (Figure 7b). Apart from this apparently unsymmetrical aspect of the anodic and cathodic signals with respect to the effect of scan rate (see the related discussion given later), our results thus indicate that the reversible oxidation potential of the highest-quality 2D J-aggregate is most likely located at 0.78 ± 0.01 V versus Ag/AgCl.

Interestingly, the shoulder-like anodic signal for the highest-quality J-aggregate turned to a distinguishable anodic peak in the case of lower-quality 2D J-aggregates of Dye 1 co-aggregated with Dye 2, as shown in Figure 8 for samples prepared at a 5/5 mixing ratio with Dye 2. This indicates that for some reason the irreversible oxidation reaction was markedly slowed for the intentionally segmented J-aggregates. Note that this reasonably accounts also for the strong broadening of the irreversible anodic peak in the slow scan mode (Figure 3). If, alternatively, there were any serious increase in the site heterogeneity for these smaller J-aggregates partitioned by Dye 2, the reversible redox peaks in the fast scan mode would also be broadened accordingly. No such tendency can be discerned in Figure 8 as compared to Figure 7.

The appearance of a distinct couple of anodic and cathodic peaks in Figure 8 allows a more straightforward analysis of the reversible potential. When the two sets of voltammograms in

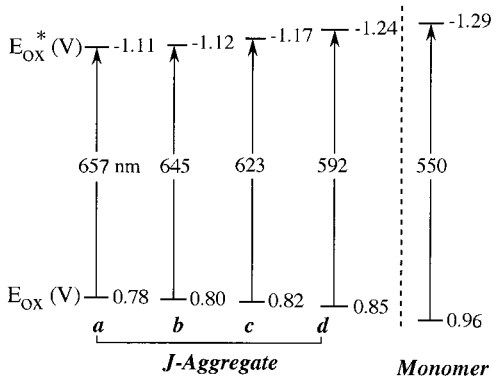

Figure 9. Energy level (in terms of oxidation potential) diagram for series of J-aggregates (a−d referring to respective J-bands in Figure 2) in comparison with that of a monomer. Vertical HOMO−LUMO transition energies (corresponding to the absorption peaks) were used to predict the excited-state oxidation potentials.

Figure 8 are compared, there is no doubt that the cathodic peak position is again much less sensitive to the scan rate than the anodic peak. We found that an approximate positional matching of the two peaks occurred at ∼0.82 V in the lower limiting scan condition of 5 V/s. We thus conclude that the reversible oxidation potential for the sample with 5/5 mixing ratio with Dye 2 is located at 0.82±0.01 V, ∼40 mV more positive than that for the highest-quality 2D J-aggregate. In a similar manner, the reversible oxidation potential for the moderately high-quality Dye 1 J-aggregate prepared with a minor mixing of Dye 2 (9/1) was estimated to be 0.80 ± 0.01 V and that for the lowest-quality Dye 1 J-aggregate (2/8) to be around ∼0.85 V. Overall, there is no doubt that the reversible oxidation potential shifts positively with decreasing aggregate size or quality. Furthermore, the position of the irreversible monomer oxidation signal (0.93−1.0 V) in the slow scan conditions, which closely fit the reversible monomer oxidation potential (0.95−0.98 V) in solution, seems to be at a reasonable extreme position in the extension of the above potential order.

Once the ground-state oxidation potential (HOMO level) is known in this way, we can immediately deduce also the excited-state oxidation potential (LUMO level) on the basis of the experimental HOMO−LUMO transition energy. One problem is that the electrochemically significant excited state should generally be in its lowest vibrational level, but the corresponding 0−0 transition energies for the series of 2D J-aggregates on Au(111) are not yet available. We found, however, that for the reference monomers of Dye 1 in solution, for which the fluorescence spectrum is readily obtained, the difference between the vertical and the 0−0 transition energies remains as small as ∼0.06 eV. The weak exciton−phonon coupling in J-aggregates as reflected in their sharp J-bands must further reduce the difference between the Franck−Condon state and the vibrationally relaxed one. Thus, for the present purpose the vertical HOMO−LUMO transition energies would suffice to predict a series of excited-state oxidation potentials. We then obtain the energy diagram (in terms of oxidation potentials) as shown in Figure 9. The systematic upward shift of the HOMO level by the J-aggregation is concomitant with the opposite (downward) shift in the LUMO level for the whole series of Dye 1 J-aggregates that considerably vary in domain size.

3.4. Energetics of Redox Level Shift. The essential energetics that controls the reversible oxidation of the 2D J-aggregate in comparison with that of the monomer can be described on the basis of the following elementary processes and the relevant energy terms:

$$\mathrm{M} + J_{n-1} \rightarrow J_n + \epsilon_\mathrm{J} \qquad (\mathrm{R}_1)$$

$$\mathrm{M}^* + \mathrm{J}_{n-1} \rightarrow \mathrm{J}_n^* + \epsilon_\mathrm{J} + \Delta\epsilon_\mathrm{J}^* \qquad (\mathrm{R}_2)$$

$$\mathrm{M}^+ + \mathrm{J}_{n-1} \rightarrow \mathrm{J}_n^+ + \epsilon_\mathrm{J} + \Delta\epsilon_\mathrm{J}^+ \qquad (\mathrm{R}_3)$$

$$\mathrm{M} + h\nu_\mathrm{M} \rightarrow \mathrm{M}^* \qquad (\mathrm{R}_4)$$

$$\mathrm{M} + I_\mathrm{M} \rightarrow \mathrm{M}^+ \qquad (\mathrm{R}_5)$$

R_1 adds one monomer to a J-aggregate with $n - 1$ monomer units, with ϵ_J simply representing the size-dependent molar cohesive energy of the 2D J-aggregate.[28] In R_2 and R_3, incorporated into the same J-aggregate is either an excited-state or an ionized monomer. R_4 and R_5 define the monomer optical absorption energy ($h\nu_\mathrm{M}$) and ionization energy (I_M), respectively. Note that it is I_M that determines the monomer oxidation potential. In a similar manner, we define the optical absorption and ionization energies of the J-aggregate by $h\nu_\mathrm{J}$ and I_J, respectively, and the excited-state ionization energies for the monomer and the J-aggregate by I_M* and I_J*, respectively. $\Delta\epsilon_\mathrm{J}$* and $\Delta\epsilon_\mathrm{J}^+$ in R_2 and R_3 are the formal correction terms for the additional cohesive energy that the J-aggregate gains as it incorporates the excited-state or ionized monomer instead of the ground-state monomer. However, at least $\Delta\epsilon_\mathrm{J}$* has a more definite physical meaning. Once M* has been incorporated into the J-aggregate, the excited-state energy no longer belongs to any single monomer site but is delocalized over the entire J-aggregate domain. Every monomer unit then will experience essentially the same cohesive energy (ϵ_J) as that in the ground-state J-aggregate, and thus, $\Delta\epsilon_\mathrm{J}$* (>0) becomes a pure representation of the exciton delocalization energy. The same story may also apply to $\Delta\epsilon_\mathrm{J}^+$ if the hole is delocalized as fast as the exciton. If, on the contrary, the holes are strongly localized to negatively affect the cohesive energy by disturbing the structural continuity of the 2D J-aggregate, $\Delta\epsilon_\mathrm{J}^+$ must include the corresponding negative term, while a dielectric stabilization of the net positively charged hole state will always positively add to $\Delta\epsilon_\mathrm{J}^+$. At any rate, it is only when $\Delta\epsilon_\mathrm{J}^+$ takes an overall positive value that we can reproduce the experimental upward shift in the HOMO level.

A total energy diagram (Figure 10a) with the species appearing in R_1−R_5 helps the whole energetics of interest to be understood more quickly. To make this diagram, we first place side-by-side the two levels for $\mathrm{M} + J_{n-1}$ and for J_n with a net energy difference, ϵ_J, according to R_1. Then by using the series of optical absorption and ionization energies defined above, automatically generate all the other relevant levels. The resultant diagram must also be consistent with the energetics described by R_2 and R_3, and in the conditions of $\Delta\epsilon_\mathrm{J}^+ > 0$ and $\Delta\epsilon_\mathrm{J}^* > \Delta\epsilon_\mathrm{J}^+$ (necessary assumptions to account for the experimental results), we obtain the relationships as shown in Figure 10a. This total energy diagram can easily be transformed to the corresponding electronic energy diagram, Figure 10b, for the ground (HOMO) and excited (LUMO) states, of which the positions are determined by their respective ionization energies, as shown in Figure 10a. It thus follows in Figure 10b that the oxidation potential of the J-aggregate is more negative by $\Delta\epsilon_\mathrm{J}^+/e$ than that of the monomer and that the difference, $(\Delta\epsilon_\mathrm{J}^*-\Delta\epsilon_\mathrm{J}^+)/e$, determines the excited-state oxidation potential of the J-aggregate relative to that of the monomer. Here e denotes the proton charge to translate the energy to the potential difference. If one assumes that the exciton delocalization energy ($\Delta\epsilon_\mathrm{J}$*) is more like an intrinsic quantity of the J-aggregate depending only on the aggregate size, then the redox levels of the J-aggregate are controlled solely by $\Delta\epsilon_\mathrm{J}^+$, i.e., by the static and dynamic

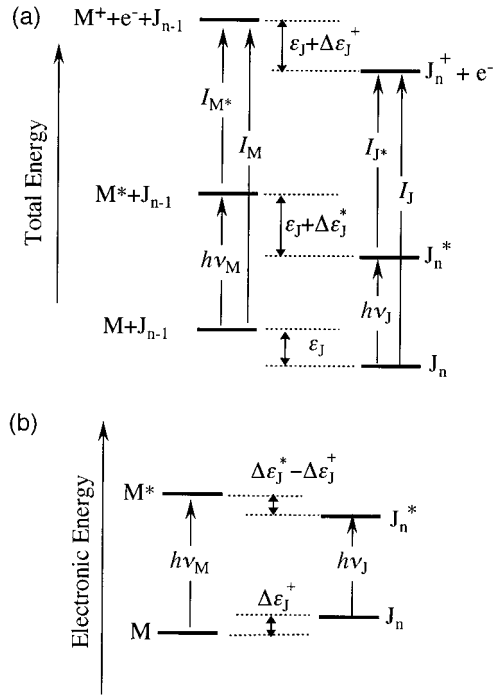

Figure 10. Total (a) and electronic (b) energy diagrams showing the origin of redox level shifts by J-aggregation. See text for construction of these diagrams and for definition of key energetic parameters.

characters of holes in the given aggregate framework and its external environment. The experimental energy diagram given in Figure 9 suggests that $\Delta\epsilon_J^+$ (>0) becomes monotonically smaller with decreasing aggregate size.

3.5. Mechanistic Details of Reversible Oxidation. It should be stressed here that even for the series of lower-quality J-aggregates, for which we found a distinguishable couple of anodic and cathodic peaks, the estimated total number of electrons transferred under each redox peak was still limited to ~15% of the total number of Dye 1 molecules on the electrode. This limitation seems to be an important consequence of the reversible J-aggregate oxidation and due probably to the energetic constraint against accumulation of too many positive holes or repulsive excess positive charges inside each J-aggregate domain. One may argue that in the voltammetric measurement any net current flow from the J-aggregate to the electrode must be balanced with the equivalent ionic current in the electrolyte solution toward the J-aggregate, and thus, the electric neutrality as a whole must be preserved at all times. Even so, it is still not easily conceivable that the repulsive force between the accumulated holes is always so well offset by the counter negative charges supplied from the electrolyte solution that any number of holes can be accumulated inside each J-aggregate domain without any energetic constraint.

One may also speculate that the reversible oxidation, in a manner similar to that of the irreversible oxidation, could have also been confined to the domain edges, thus involving the corresponding limited number of dye molecules. Were this the case, the lower-quality J-aggregates with smaller domain sizes (hence with larger fractions of dye molecules located along the domain edges) would facilitate higher levels of partial reversible oxidation. This does not agree with the aforementioned experimental results. Furthermore, ~15% is probably the maximum fraction of dye molecules locatable along the domain edges for the highest-quality 2D J-aggregates. The above alternative interpretation requires all of them to be reversibly oxidized to account for the intensity of the reversible cathodic signal. The resulting local repulsive force between the holes that are so densely segregated along the domain edges must be quite significant.

The same problem as discussed above also seems to have an important kinetic relevance for the unsymmetrical scan-rate dependence of the anodic and cathodic signals noted earlier. According to the general expression of linear-sweep voltammograms in a diffusionless system,[19,20] unsymmetrical positioning of the anodic and cathodic peaks with respect to the reversible potential may occur whenever the so-called transfer coefficient deviates significantly from 0.5. However, the almost unilateral shift of the anodic peak in the scan conditions yielding the potential difference only ~60 mV or less between the two peaks hardly conforms to that general scheme. Normally, the occurrence of redox peaks in a linear-sweep voltammogram is associated with a depletion of reduced or oxidized species in the course of the relevant electrode reaction. The situation is certainly not that simple for the anodic peak produced under the proposed limitation or energetic constraint against an excess charge transfer. The peak position in this case will also depend on how efficiently the resulting positive charges are externally compensated by the electrolyte anions. The cathodic peak, on the other hand, arises from a finite concentration of positive holes that have accumulated during the anodic scan and reaccept electrons to restore the fully reduced state and thus at least formally resembles the common cathodic peaks in liner-sweep voltammograms. Thus, the partial reversible oxidation of the 2D J-aggregate seems to inherently entail an unsymmetrical nature.

Apart from the exact origin of the unsymmetrical shifts of the anodic and cathodic peaks, their small separation of ~60 mV at the maximum scan rate of 100 V/s or, alternatively, the very small shift of the cathodic peak potential in the given range of scan rates points to a considerably large electron-transfer rate for the significant tunneling gap of ~13 Å. According to the expression given by Laviron,[19,20] the 60 mV peak separation at 100 V/s leads to a unimolecular rate constant of the electron transfer (at the standard potential), $\sim 2 \times 10^3\ s^{-1}$, in a broad range of transfer coefficient around 0.5. This high electron-transfer rate can be attributed to a minor reorganization energy associated with the reversible J-aggregate oxidation, together with a continuum of electronic states in the gold electrode.

Other important mechanistic issues that remain to be clarified are how the reversible oxidation is correlated with the irreversible one and why the irreversible reaction was so much slowed for the intentionally segmented J-aggregates. The irreversible oxidation may involve a similar one-electron oxidation step as that in the reversible oxidation, the resulting holes then participating in the follow-up irreversible reaction. For this mechanism to be compatible with the strong preference for the domain edges in the irreversible reaction, the holes must be so mobile (not necessarily as fast as excitons) that they can easily diffuse out to the domain edges. Then possible differences in such dynamic characters of holes between aggregates with different domain sizes or levels of structural perfection may have something to do with the remarkably different kinetics of irreversible oxidation; the point requires further studies for clarification.

4. Conclusions

A self-assembled cysteamine monolayer on an atomically flat Au(111) allows controlled layering of 2D J-aggregates of anionic cyanine dyes at a fixed distance ~13 Å above the Au(111) surface. This provides a superior model electrode system for

directly investigating the unique redox properties of layered J-aggregates as a function of the aggregate size.

All the cyclic voltammograms of the 2D J-aggregate obtained in widely ranging scan conditions can be satisfactorily explained by the combination of a reversible one-electron oxidation producing potentially mobile holes and an irreversible oxidation in which several extra electrons/molecule are transferred to the gold electrode. The decay of the J-band caused by the irreversible oxidation was accompanied by negligibly small changes in its shape and sharpness, pointing to the characteristic mode of irreversible reaction involving the domain edges as the preferential reaction sites.

The reversible one-electron oxidation signal could be more-or-less clearly separated from that representing the irreversible oxidation reaction by the fast-scan voltammetry, yielding either a shoulder-like or a distinguishable anodic peak followed in the reverse scan by a well-defined cathodic peak. The total number of electrons transferred under each peak was limited to ∼15% of the total dye molecules supported on the electrode, which we relate to energetic constraint against accumulation of too many repulsive positive holes.

The standard oxidation potentials of a series of 2D J-aggregates that significantly differ in domain size and structural quality ranged from ∼0.78 V (for the highest-quality J-aggregate) to ∼0.85 V (for the lowest-quality J-aggregate) versus Ag/AgCl, and they were invariably more negative than the monomer oxidation potential expected to lie at ∼0.96 V. The large spectral red shift from the monomer band characteristic of the J-aggregate is thus concomitant with cooperative upward and downward shifts in the HOMO and the LUMO level, respectively. The effect of the J-aggregation on the redox levels critically depends on the nature of positive holes in the given aggregate framework.

References and Notes

(1) Bohn, P. W. *Annu. Rev. Phys. Chem.* **1993**, *44*, 37.
(2) Möbius, D. *Adv. Mater.* **1995**, *7*, 437.
(3) Daehne, S.; De Rossi, U.; Moll, J. *J. Soc. Photogr. Sci. Technol. Jpn.* **1996**, *59*, 250.
(4) Kobayashi, T., Ed. In *J-Aggregates*; World Scientific: Singapore, 1996
(5) Eachus, R. S.; Marchetti, A. P.; Muenter, A. A. *Annu. Rev. Phys. Chem.* **1999**, *50*, 117.
(6) West, W.; Gilman, P. B. In *The Theory of the Photographic Process*, 4th ed.: James, T. H., Ed.; Macmillan: New York, 1977; Chapter 10.
(7) Lenhard, J. *Imaging Sci.* **1986**, *30*, 27.
(8) Tani, T.; Ohzeki, K.; Seki, K. *J. Electrochem. Soc.* **1991**, *138*, 1411.
(9) Lenhard, J. R.; Hein, B. R. *J. Phys. Chem. B* **1996**, *100*, 17287.
(10) Sato, T.; Yamamoto, A.; Kawasaki, M. *Chem. Lett.* **2000**, 394.
(11) Kawasaki, M.; Sato, T.; Yoshimoto, T. *Langmuir* **2000**, *16*, 5409.
(12) Caldwell, W. B.; Chen, K.; Mirkin, C. A.; Babinec, S. J. *Langmuir* **1993**, *9*, 1945.
(13) Willner, I.; Riklin, A. *Anal. Chem.* **1994**, *66*, 1535.
(14) Chen, H.-Y.; Zhou, D.-M.; Xu, J.-J.; Fang, J.-Q. *J. Electroanal. Chem.* **1997**, *422*, 21.
(15) Yu, H. Z.; Zhao, J. W.; Wang, Y. Q.; Cai, S. M.; Liu, Z. F. *J. Electroanal. Chem.* **1997**, *438*, 221.
(16) Ruan, C.; Yang, R.; Chen, X.; Deng, J. *J. Electroanal. Chem.* **1998**, *455*, 121.
(17) Mirkhalaf, F.; Schiffrin, D. J. *J. Chem. Soc., Faraday Trans.* **1998**, *94*, 1321.
(18) Berggeren, C.; Stalhandske, P.; Brundell, J.; Johansson, G. *Electroanalysis* **1999**, *11*, 156.
(19) Laviron, E. *J. Electroanal. Chem.* **1979**, *100*, 263.
(20) Laviron, E. *J. Electroanal. Chem.* **1979**, *101*, 19.
(21) Bard, A.J.; Faulkner, L. R. *Electrochemical Methods, Fundamentals and Applications*; John Wiley & Sons: New York, 1980.
(22) Widrig, C. A.; Chung, C.; Porter, D.J. *Electroanal. Chem.* **1991**, *310*, 335.
(23) Everett, W. R.; Welch, T. L.; Reed, L.; Fritsch-Faules, I. *Anal. Chem.* **1995**, *67*, 292.
(24) Kawasaki, M.; Ishii, H. *Langmuir* **1995**, *11*, 832.
(25) Kawasaki, M.; Uchiki, H. *Surf. Sci.* **1997**, *388*, L1121.
(26) Kawasaki, M. *Appl. Surf. Sci.* **1998**, *135*, 115.
(27) Lanzafame, J. M.; Muenter, A. A.; Brumbaugh, D. V. *Chem. Phys.* **1996**, *210*, 79.
(28) Kawasaki, M.; Inokuma, H. *J. Phys. Chem. B* **1999**, *103*, 1233.
(29) The apparent shape of the Dye 2 J-band in Figure 2, with distinct tailing on the longer wavelength side, is not really associated with the Dye 2 J-aggregate. The optical constants of gold change rapidly in the spectral region shorter than ∼520 nm; thereby, the high reflectance characteristic of metal drops seriously. In such a spectral region, the reflection absorbance defined in the text no longer simply scales to the absorption coefficient of thin adsorbates on the metal, as confirmed by a numerical simulation of the reflectance based on the Fresnel formula.
(30) Sabatani, E.; Rubinstein, I. *J. Phys. Chem.* **1987**, *91*, 6663.
(31) French, M.; Creager, S. E. *Langmuir* **1998**, *14*, 2129.
(32) When taken after the irreversible anodic scan, the intensity of XPS signals arising from the S, N, and Cl atoms associated with the dye molecules, which are probably stuck to the irreversibly oxidized dye remains as well, dropped by at least 70%.